



Research Paper

Controlled synthesis of upconverting nanoparticles/ $Zn_xCd_{1-x}S$ yolk-shell nanoparticles for efficient photocatalysis driven by NIR light



Wan-Ni Wang^a, Chen-Xi Huang^a, Chen-Yang Zhang^a, Meng-Li Zhao^a, Jun Zhang^a, Hua-Jian Chen^a, Zheng-Bao Zha^a, Tingting Zhao^{b,*}, Hai-Sheng Qian^{a,*}

^a School of Biological and Medical Engineering, School of Food Science and Engineering, Hefei University of Technology, Hefei, 230009, PR China

^b Institute of Intelligent Machines, Chinese Academy of Sciences, Hefei, 230031, PR China

ARTICLE INFO

Keywords:

Upconversion nanoparticle
Semiconductor
Yolk-shell
Photocatalysis

ABSTRACT

Photocatalysts driven by near infrared light (NIR) are of great importance for making full use of solar energy and wide applications in biomedicine, biosensor, photocatalysis, and etc. In this work, we demonstrate a facile template assisted hydrothermal approach to fabricate upconversion nanoparticles (UCNPs) and $Zn_xCd_{1-x}S$ yolk-shell nanoparticles, although the yolk-shell nanoparticles were made from hexagonal phase of $\beta\text{-NaYF}_4$ ($\text{NaYF}_4\text{:Yb/Tm@NaYF}_4\text{:Yb/Er}$) and II–VI semiconductor materials with a large lattice mismatch of more than 10%. The growth mechanism of the formation of yolk-shell nanostructures has been extensively investigated and the shape evolution with the time has been demonstrated. Steady and dynamic fluorescence spectra show that the as-prepared yolk-shell nanoparticles of UCNPs/ $Zn_xCd_{1-x}S$ can be used as efficient nanotransducer for NIR light owing to enhanced energy transfer efficiency. Interestingly, the as-prepared yolk-shell nanoparticles exhibit excellent photocatalytic performance on degradation towards RhB dyes, excellent biocompatible properties and high production ability for hydroxyl radical ($\cdot\text{OH}$) and single oxygen ($^1\text{O}_2$), which might be employed to wide applications in solar cell, hydrogen production, and photodynamic therapy related nano-biotechnology.

1. Introduction

Photocatalysis has been recognized as one of the most important approaches to overcome the worldwide energy crisis and environmental pollution issues [1]. In particular, photocatalysis driven by near infrared (NIR) light has attracted much attention because NIR light accounts for more than 40% of solar energy [2–7]. Lanthanide ions doped upconversion nanoparticles (UCNPs) can efficiently convert low-energy photons in the NIR region to high-energy photons in the visible region [8–12]. In recent years, constructing fluorescence resonance energy transfer (FRET) systems using UCNPs as nanotransducer of NIR light has been extensively studied owing to their fantastic applications in photocatalysis, sensor solar cell, detection and bio-nanotechnology [13–21]. In general, the FRET systems are incorporated with acceptor and donor in close proximity, in which more overlap of the fluorescence spectrum of donor and absorption spectrum of the acceptors will result in higher energy transfer efficiency. Among various fluorescent donors, such as organic dye, quantum dots and semiconductors, UCNPs with unique upconversion fluorescence property are known as FRET donors driven by near infrared light via FRET or irradiation energy transfer process [22–27]. Up to date, the FRET systems incorporated with

UCNPs (donors) and acceptors including dyes, CdTe, CdS, ZnO and some complex nanostructures have drawn considerable research interest [28–30]. Semiconductor (II–VI) as an efficient acceptor exhibits wide absorption and tunable emission and excitation wavelength for the FRET systems. However, it is a challenging task for constructing FRET systems by incorporating UCNPs with semiconductors in closer proximity due to their large lattice mismatch.

Currently, much effort has been paid to synthesize the UCNPs based hetero-structures including UCNPs/SiO₂ [31–33], UCNPs/CdSe [34], UCNPs/CdS [35], UCNPs/TiO₂ [36–39], UCNPs/ZnO [40] and UCNPs/CdS/TiO₂ [41,42] and so on. To fabricate this UCNPs based FRET systems, high temperature thermal decomposition method, hydrothermal method, electro-spinning and chemical assembly have been developed, among which electro-spinning technique was regarded as an alternative method for fabrication composites by incorporating with multi-components in close proximity on large scale. However, the distance of the UCNPs and semiconductor is still hard to be controlled using electro-spinning method, leading to the reduced energy transfer efficiency. Additionally, an appropriate lattice matching is necessary for heterojunction of different inorganic nanomaterials. In particular, solution method can provide a facile and mild condition for chemical reaction to

* Corresponding authors.

E-mail addresses: tingtingzhao2014@sina.cn (T. Zhao), shqian@hfut.edu.cn (H.-S. Qian).

achieve unique nanostructures with well controlled size, morphologies and chemical or physical properties. Up to date, it's a hot research topic for solution synthesis of core-shell nanoparticles of UCNPs and semiconductors including ZnS, CdS and CdSe with more than 10% of the lattice mismatching degree between the two components.

Compared to single part of ZnS or CdS, alloyed $Zn_xCd_{1-x}S$ nanostructures show strong redox ability and good photo-corrosion resistance, which can enhance the separation efficiency of photo-generated hole and electrons greatly [43,44]. Herein, in this communication, we report a facile template assisted hydrothermal approach to fabricate the yolk-shell nanostructured composites combined up-converting nanoparticles and alloyed $Zn_xCd_{1-x}S$. The growth mechanism of the formation of yolk-shell nanoparticles has been carefully investigated. The steady and dynamic state fluorescence spectra of the as-prepared UCNPs@ $Zn_xCd_{1-x}S$ nanoparticles exhibit that the energy transfer efficiency has been enhanced greatly compared with the composites of TiO_2 /UCNPs/CdS nanofibers [39]. Additionally, the as-prepared UCNPs@ $Zn_xCd_{1-x}S$ nanoparticles show good biocompatibility and chemical stability, which is of great importance to apply in wastewater treatment, energy conversion and photodynamic therapy of cancer cells.

2. Materials and methods

All chemicals were used as received and without further purification. Sodium hydroxide (NaOH, 96 wt%), ammonium fluoride (NH_4F , 98 wt%), rare earth chlorides hexahydrate ($YCl_3 \cdot 6H_2O$, $YbCl_3 \cdot 6H_2O$, $TmCl_3 \cdot 6H_2O$, $ErCl_3 \cdot 6H_2O$, 99.99%), cadmium acetate dihydrate ($C_4H_6CdO_4 \cdot 2H_2O$), 9, 10-Anthracenediylbis (methylene) dimalonic acid (ABDA) and rhodamine B (RhB) were purchased from Aladdin Industrial Corporation. Hexadecyltrimethylammonium bromide (CTAB, 99.9 wt%) and terephthalic acid (TAOH) were purchased from Adamas Reagent Co. Ltd. Zinc nitrate hexahydrate ($Zn(NO_3)_2 \cdot 6H_2O$, 99.0 wt%), 1-ascorbic acid (AA, 99.7 wt%), methanol (CH_3OH , 99.5 wt%), thiourea (H_2NCSNH_2 , 99.0 wt%) and hexamethylenetetramine (HMTA, 99.0 wt%) were purchased from Sinopharm Chemical Reagent Co. Ltd. $NaYF_4 \cdot Yb(30\%) \cdot Tm(0.5\%) \cdot Er(2\%)$ core-shell nanoparticles (abbreviated as UCNPs) had been prepared via the sequential growth protocol reported by our group [45]. Hydrophilic UCNPs have been achieved by epitaxial growth of ZnO. Hydrophilic UCNPs were prepared via a modified surfactant encapsulation techniques reported by Fan's group [46].

2.1. Fabrication of UCNPs@AA-[$Zn(OH)_4$]²⁻ core-shell nanoparticles

The synthetic procedure for the UCNPs@AA-[$Zn(OH)_4$]²⁻ core-shell nanoparticles was modified according to the reported protocol [40]. Briefly, 1 mmol $Zn(NO_3)_2 \cdot 6H_2O$ and HMTA with an equal molar amount were added into 50 mL aqueous solution containing 0.3 mmol of CTAB and 0.2 mmol of AA under magnetic stirring to form clear solution. Subsequently, 1.8 mL of as-prepared hydrophilic UCNPs (ca. 0.63 mg) was added by dropwise into the previous clear solution and stirred for 5 min. The mixture was heated and kept at 85 °C for 10 h. The final product was collected by centrifugation and washed with distilled water and absolute ethanol for several times.

2.2. Synthesis of UCNPs@ $Zn_xCd_{1-x}S$ yolk-Shell nanoparticles

Before the synthesis of UCNPs@ $Zn_xCd_{1-x}S$ (Zn and Cd core-shell nanoparticles under hydrothermal process), the UCNPs@ZnS core-shell nanoparticles were synthesized by a sulfidation process. The conversion from the as-prepared UCNPs@AA-[$Zn(OH)_4$]²⁻ core-shell nanoparticles to UCNPs@ZnS core-shell nanoparticles was carried out in a simple self-made sulfidation apparatus using H_2S gas. In a typical synthesis process, 0.2 g UCNPs@AA-[$Zn(OH)_4$]²⁻ core-shell nanoparticles were heated to 50 °C and H_2S gas was introduced into the

reaction vessel and kept at 50 °C for 4 h.

The composition of the UCNPs@ $Zn_xCd_{1-x}S$ core-shell nanoparticles can be tunable by changing the molar ratio of the Zn and Cd. In a typical protocol of UCNPs@ $Zn_xCd_{1-x}S$ yolk-shell nanoparticles, 0.12 mmol UCNPs@ZnS and 0.12 mmol cadmium acetate were added into 10 mL of deionized water to form clear solution with vigorous stirring, and then 6 mmol thiourea were added into the solution and stirred for 30 min at room temperature. Subsequently, the solution was then transferred into a 30 mL Teflon-lined stainless-steel autoclave and maintained at 140 °C for 2 h. The final product was collected by centrifugation and washed several times with distilled water and ethanol to remove the residual cations and anions. The precipitate was dried at 60 °C for 6 h. The mole ratio of Zn/Cd (0.45/0.55) has been accurately determined using atomic absorption spectroscopy (AAS). For comparison, UCNPs@ $Zn_xCd_{1-x}S$ ($x = 0.28, 0.35, 0.64$) samples have been synthesized according to the same protocol and the x value was determined using atomic absorption spectroscopy.

2.3. Hydroxyl radical ($\cdot OH$) detection

Terephthalic acid (TAOH) was used as a standard reagent to investigate the production of $\cdot OH$. Typically, 0.4 g NaOH and 0.8307 g TAOH were added into 50 mL double distilled water and dissolved to form clear solution. And then, 15 mg of as-prepared UCNPs@ $Zn_{0.45}Cd_{0.55}S$ yolk-shell nanoparticle was added into the solution. The solution was irradiated using a Xe lamp with an UV-vis filter for 30 min under magnetic stirring. The solution was determined on an Edinburgh FLS980 fluorescence spectrometer after removal of the yolk-shell nanoparticle by centrifugation.

2.4. Singlet oxygen (1O_2) detection

The 9, 10-Anthracenediylbis (methylene) dimalonic acid (ABDA) was used as a standard to investigate the production of singlet oxygen. The 200 μ L of UCNPs@ $Zn_xCd_{1-x}S$ solution (1 mg/mL) was added in 2 mL of phosphate buffered saline (PBS) (0.1 M, pH 7.4) mixed with 200 μ g ABDA. The mixture was kept after equilibrium for 1 h in dark and irradiated with 980 nm NIR laser at 10 min interval. After that, the absorption intensity at 379 nm of ABDA was measured by a Hitachi U-5100 spectrophotometer.

2.5. Characterizations

The surface morphologies of these products were investigated using field-emission scanning electron microscopy (FESEM) with a SU8020 (Hitachi, Japan), transmission electron microscopy (TEM) images, high-resolution transmission electron microscopy (HRTEM), and energy-dispersive X-ray (EDX) operated with JEM-2100F (JEOL, Japan), respectively. The X-ray diffraction (XRD) patterns of the as-prepared samples were obtained by an X'Pert PRO MPD X-ray diffractometer (PANalytical B.V., Holland) with use of graphite monochromated Cu K α radiation. The UV-vis absorption spectra of the as-prepared samples were obtained using a Hitachi U-5100 spectrophotometer (Hitachi High-Technology Corporation) and all the samples were dispersed in double distilled water. The UV-vis diffuse reflectance spectra (DRS) of the as-prepared solid samples were investigated by using a CARY 5000 (Agilent Technology Corporation). X-ray photoelectron spectra (XPS) were operated on an ESCALAB250Xi X-ray photoelectron spectrometer (Thermo Scientific, American). Upconversion fluorescent spectra were measured on an Edinburgh FLS980 fluorescence spectrometer using an external CW laser of 980 nm. Atomic absorption spectroscopy (AAS) was used to determine the mole ratio of Zn/Cd, which was carried out using AA800 (Perkin Elmer, American).

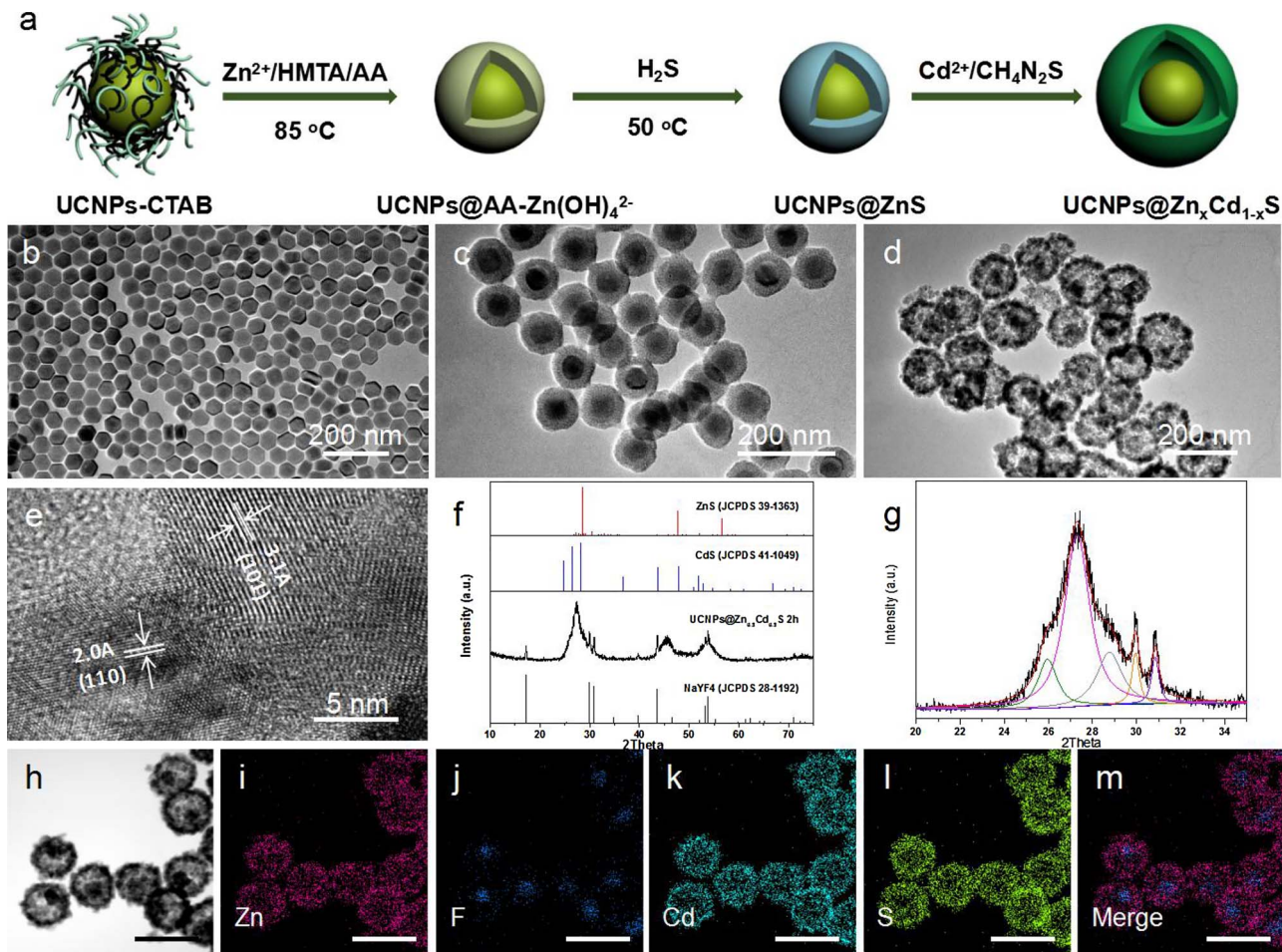


Fig. 1. (a) Schematic illustration of the synthetic procedure of UCNPs@Zn_xCd_{1-x}S yolk-shell nanoparticles. (b, c) TEM images of NaYF₄:Yb/Tm@NaYF₄ upconversion nanoparticles and UCNPs@AA-[Zn(OH)₄]²⁻ core-shell nanoparticles, respectively. (d, e) TEM and high resolution TEM images of UCNPs@Zn_xCd_{1-x}S nanoparticles. (f, g) XRD patterns of the UCNPs@Zn_xCd_{1-x}S yolk-shell nanoparticles. (h) STEM images of the UCNPs@Zn_xCd_{1-x}S yolk-shell nanoparticles. (i-m) STEM elemental mappings of Zn, F, Cd, S, and merged image of Zn and F elements in (h). All the scale bars in Fig. 1h-m are 200 nm.

3. Results and discussion

As illustrated in **Fig. 1a**, UCNPs@AA-[Zn(OH)₄] complex core-shell was firstly prepared by coating a layer of AA-[Zn(OH)₄] complex at the surface of upconversion nanoparticles [40], which can be transferred to the UCNPs@ZnS core-shell nanoparticles via a sulfidation process using H₂S. As shown in **Fig. S1 (Supporting Information)**, the scanning transmission electron microscopy (STEM) image and elemental mapping images show that the UCNPs@ZnS core-shell nanoparticles have been obtained with similar size and morphologies, demonstrating the synthesis of UCNPs@ZnS successfully. UCNPs@Zn_xCd_{1-x}S yolk-shell nanoparticles were subsequently synthesized by using thiourea and Cd (Ac)₂ in the presence of UCNPs@ZnS core-shell nanoparticles under hydrothermal condition (at 140 °C). **Fig. 1b** shows the transmission electron microscopy (TEM) image of hydrophilic NaYF₄:Yb/Tm@NaYF₄:Yb/Er nanoparticles (abbreviated as UCNPs) with an average size of 42 nm in diameter, which have been synthesized via a sequential growth process previously reported by our group [45]. As shown in **Fig. 1c**, the as-prepared UCNPs@AA-[Zn(OH)₄]²⁻ complex core-shell nanoparticles were 100 nm with the shell thickness of 22 nm. **Fig. 1d** shows the TEM image of the final product UCNPs@Zn_xCd_{1-x}S yolk-shell nanoparticles obtained from 0.12 mmol UCNPs@ZnS and 0.12 mmol cadmium acetate at 140 °C for 2 h, which have a uniform diameter of about 150 nm with core size of 40 nm and 5 nm in shell thickness. The high resolution transmission electron image shown in **Fig. 1e** was taken from the edge of the shell of the yolk-shell nanoparticles, in which the

lattice fringes of 3.1 and 2.0 Å are assigned to (101) and (110) crystal plane of hexagonal phase of Zn_xCd_{1-x}S; which is a little smaller than that of CdS, indicating Zn ions doped into the CdS lattices [47]. As shown in **Fig. 1f**, all the sharp X-ray diffraction (XRD) peaks can be assigned to the hexagonal phase of NaYF₄ (JCPDS No. 28-1192). In addition, three peaks located at 25.96, 27.3 and 28.78° can be derived from the wide diffraction peak located at 27° in **Fig. 1g**, which has fitted a Gaussian curve from the XRD pattern. It's worth to note that the three Gaussian peaks were slightly higher than that of corresponding diffraction peaks for pure phase of CdS, indicating the Zn ions doped CdS lattice to form alloyed Zn_xCd_{1-x}S nanostructures. The scanning transmission electron microscopy (STEM)-energy dispersive spectra (EDS) analysis has been carried out to characterize the chemical composition of the as-prepared yolk-shell nanoparticles. As shown in **Fig. 1i-l**, the elemental mapping images of the as-prepared yolk-shell nanoparticles demonstrate that the Zn, Cd, and S elements distribute homogeneously in the shell layer. In contrast, the F element distribute in the inner core of the yolk-shell nanoparticles, which can be clearly observed by the merged image of the Zn and F (**Fig. 1m**). Energy dispersive X-ray (EDX) spectra of the as-prepared product has been shown in **Fig. S2 (Supporting Information)**, indicating the co-existence of Cd, Zn, S, Y, Yb and F elements in the as-prepared yolk-shell nanoparticles. The chemical composition has been calculated and listed in **Table S1** according to the EDX spectra, and the mole ratio of Zn/Cd is 0.39/0.61. The accurate mole ratio of Zn/Cd is 0.45/0.55, which is determined by AAS. The X-ray photoelectron spectroscopy of the UCNPs@Zn_xCd_{1-x}S yolk-

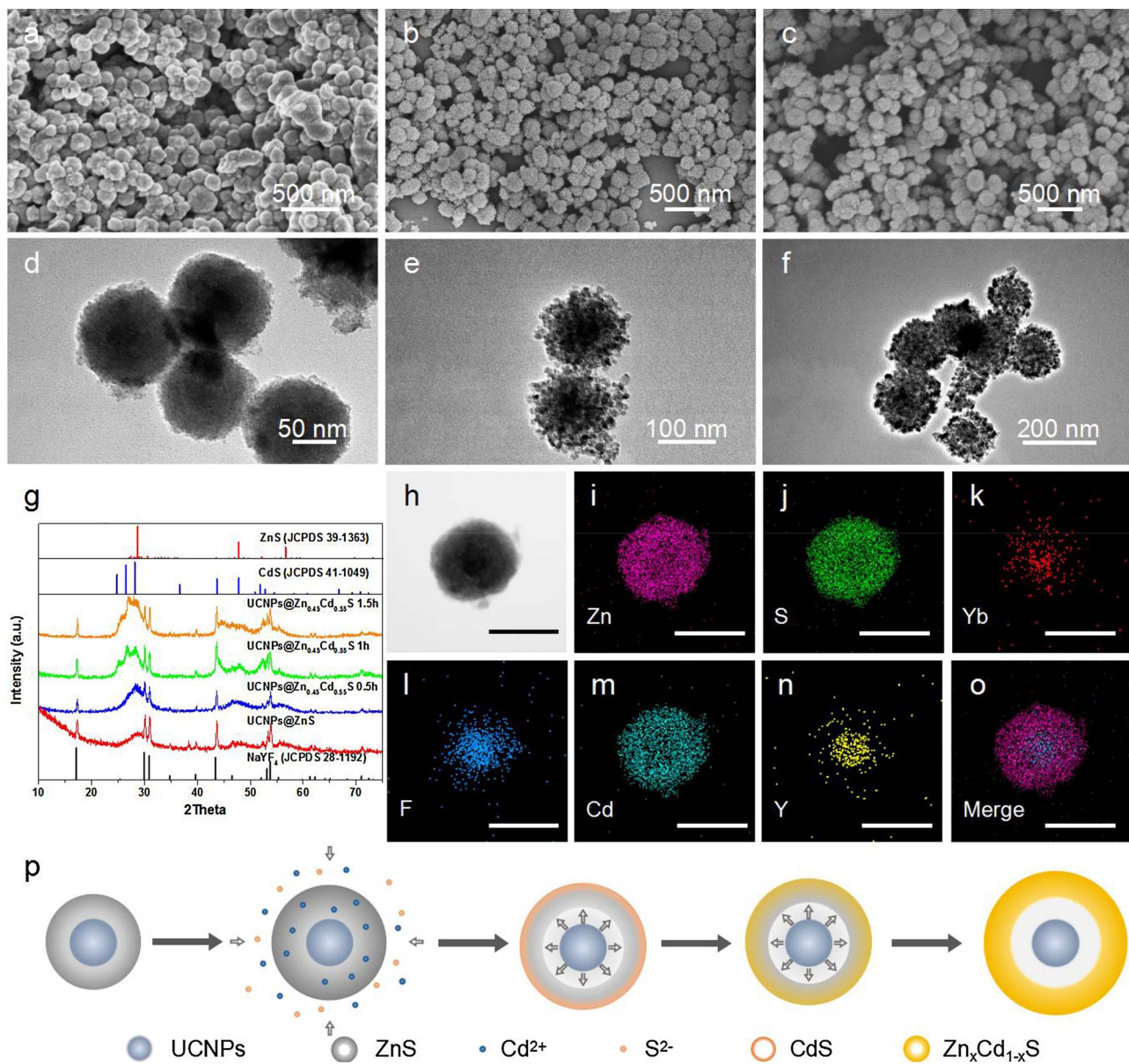


Fig. 2. (a-f) Field emission scanning electron microscopy (FESEM) and TEM images of the products obtained at different stages during the formation of yolk-shell nanostructures process. The corresponding reaction times are (a, d) 0.5 h; (b, e) 1.0 h; (c, f) 1.5 h. (g) XRD patterns of the products obtained at different stages shown in Fig. 2a-f. (h-o) Scanning transmission electron microscopy (STEM) images of the nanoparticle shown in Fig. 2d and elemental mappings of Zn, S, Na, F, Cd, Y elements and merged image of Zn and F elements in (h). Scale bars are 100 nm. (p) Schematic illustration the formation mechanism of the yolk-shell nanostructures.

shell nanoparticles (Fig. S3, Supporting Information) verified the presence of Zn, Cd, S and Y elements. The two peaks centered at 1022.3 and 1045.6 eV (Fig. S3b, Supporting Information) are corresponding to Zn 2p_{3/2} and Zn 2p_{1/2} of Zn²⁺ ions >, respectively. The peaks located at 405.0 and 411.7 are assigned to the Cd 3d of Cd²⁺ ions. The binding energy located at 1070.9 and 186.1 eV are attributed to the binding energy of Na 1s, and Er 4d (Fig. S3e,f, Supporting Information), respectively, which is very weak to be observed because the UCNPs embedded in the yolk-shell nanostructures [48–50].

The morphologies evolution for the product at early stages is used to illustrate the possible growth mechanism for the formation of UCNPs@Zn_{0.45}Cd_{0.55}S yolk-shell nanoparticles. Fig. 2a-f show the FESEM and TEM images of the product collected at 140 °C for 0.5, 1.0 and 1.5 h during the reaction of thiourea and Cd(Ac)₂ in the presence of UCNPs@ZnS core-shell nanoparticles. The sample obtained at early stage (0.5 h) was with bigger size and dense shell layers on the surface of UCNPs@ZnS core-shell nanoparticles (Fig. 2d), demonstrating that a thin layer

of CdS has been formed on the outside of the UCNPs@ZnS core-shell nanoparticles. There is no doubt about the CdS formed at the early stage under 140 °C using cadmium acetate and thiourea as reagents. Moreover, Cd²⁺ was doped into the ZnS layers at the same time, which made the shell layer with a dense aggregation of small nanoparticles. The XRD patterns of the samples obtained at early stage have been shown in Fig. 2g, in which the three wide diffraction peaks assigned to the ZnS has been shifted to lower diffraction angles, demonstrating ZnS layer doped by Cd²⁺. In Fig. 2h-o, the elemental mapping images of the as-prepared yolk-shell nanoparticles indicate that the Zn, Cd and S elements distribute homogeneously in the shell layers. With the prolonging of the reaction time, smaller ZnS or Cd²⁺ doped ZnS nanoparticles in inner layer would gradually dissolve and associated crystallization on the surface of CdS thin layers at the outmost via a diffusive mass transport process to form void space between the UCNPs and CdS layers (Fig. 2f). At the meanwhile, the CdS layer formed at outmost layer would be doped with Zn²⁺ to formed Zn_xCd_{1-x}S alloyed

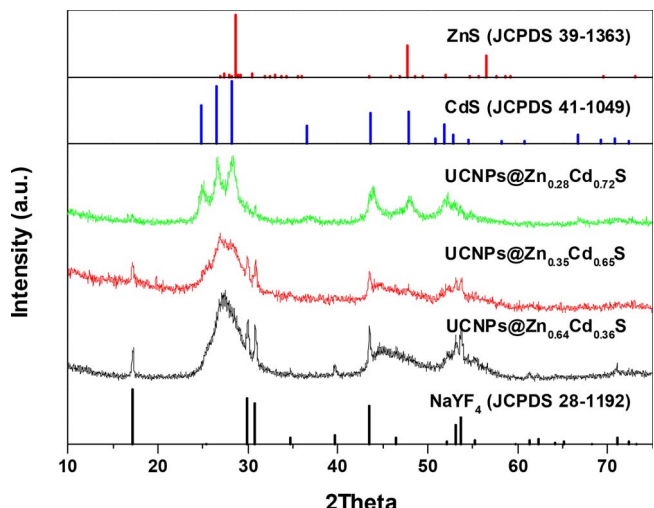


Fig. 3. X-ray diffraction patterns of the as-prepared samples shown in Fig. S4 (UCNPs@Zn_{0.28}Cd_{0.72}S, UCNPs@Zn_{0.35}Cd_{0.65}S and UCNPs@Zn_{0.64}Cd_{0.36}S).

layers via a re-crystallization process.

A possible growth mechanism has been proposed and summarized in Fig. 2p, illustrating the formation process of yolk-shell nanostructures of UCNPs@Zn_xCd_{1-x}S. Therefore, the amount of Cd(Ac)₂ will play an important role in the formation of yolk-shell nanostructures

according to the growth mechanism shown in Fig. 2p. It's clearly observed that there are no yolk-shell nanoparticles formed in absence of Cd(Ac)₂ (Fig. S4, supporting information). When the amount of Cd(Ac)₂ was reduced to 0.06 mmol, the formed yolk-shell nanostructures were not stable and some of them were collapsed easily owing to the ultrathin layers of CdS formed at early stage, as shown in (Fig. S5a, b, Supporting Information). As expected, the shell thickness become thicker to form core-shell nanoparticles of UCNPs@Zn_xCd_{1-x}S when the amount of Cd(Ac)₂ was increased to 0.24 mmol (Fig. S5e, f, Supporting Information). All these experimental results illustrated that the proposed growth mechanism in Fig. 2p is reasonable. In particular, the composition of the shell components could be tuned by adjusting the amount of Cd(Ac)₂ and the changing of 2 theta value for the X-ray diffraction peaks verify the changing of the mole ratio of Zn/Cd (Fig. 3).

The fluorescence spectra for the as-obtained UCNPs, UCNPs@ZnS, UCNPs@AA-[Zn(OH)₄]²⁻ core-shell nanoparticles and UCNPs@Zn_xCd_{1-x}S yolk-shell nanoparticles have been studied and shown in Fig. 4a. Interestingly, compared to UCNPs, UCNPs@ZnS and UCNPs@AA-[Zn(OH)₄]²⁻ complex core-shell nanoparticles, the fluorescence emissions of ¹I → F₄, ¹D → F₄, ¹D → H₆ and ¹G → H₆ of Tm³⁺ for the as-prepared UCNPs@Zn_xCd_{1-x}S (x = 0.28, 0.35 and 0.45) yolk-shell nanoparticles have been greatly quenched under the excitation of a 980 nm continuous wave (CW) laser even though the large void space exist between the UCNPs and Zn_xCd_{1-x}S components. Additionally, the transitions of ²H_{11/2} → ⁴I_{15/2} and ⁴S_{3/2} → ⁴I_{15/2} of Er³⁺ have also been quenched, showing the enhanced fluorescence energy transferring efficiency for the yolk-shell nanostructures, which is attributed to the

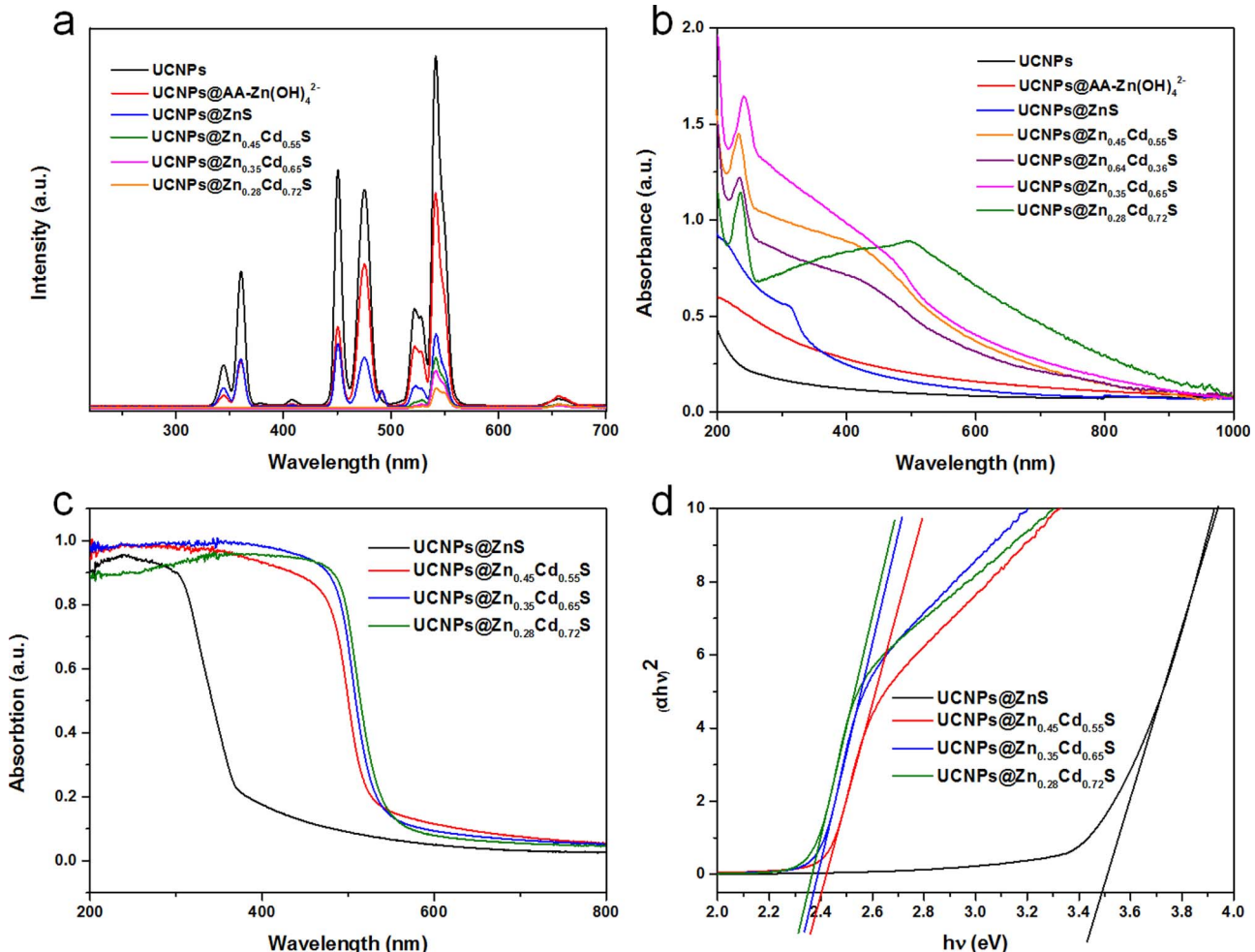


Fig. 4. (a, b) UV-vis absorbance (a) and fluorescence spectra (b) of UCNPs, UCNPs@AA-[Zn(OH)₄]²⁻ core-shell nanoparticles and UCNPs@Zn_xCd_{1-x}S yolk-shell nanoparticles dispersed in ethanol solution. (c, d) UV-vis diffuse reflectance spectra (DRS) (c) and Kubelka-Munk plots (d) for the band gap energy estimation for the different UCNPs@Cd_xZn_{1-x}S nanoparticles.

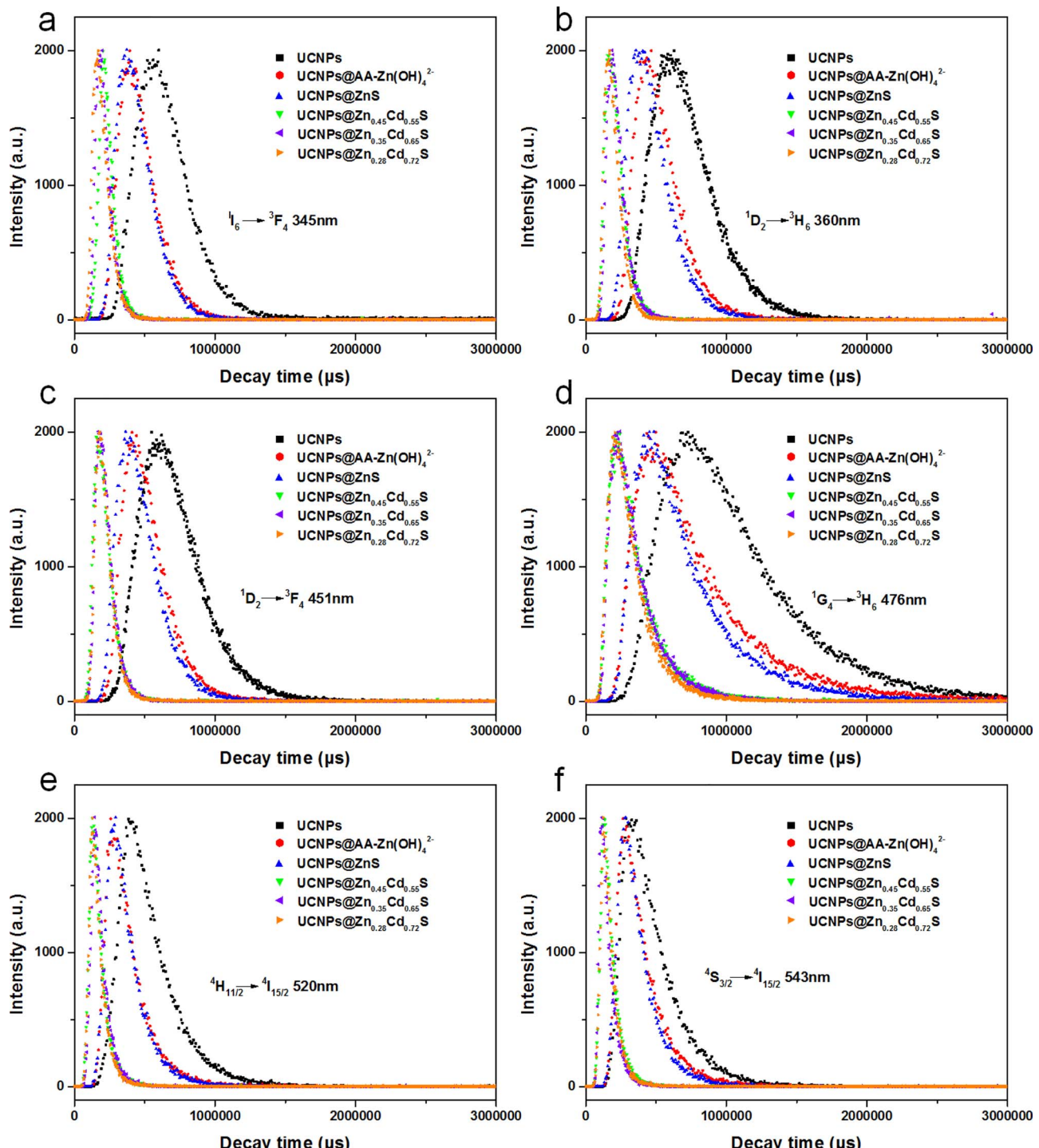


Fig. 5. (a-f) The luminescence decays of the excited state levels of Tm³⁺ (a-d) and Er³⁺ (e, f) for the UCNPs, UCNPs@AA-[Zn(OH)₄]²⁻ and UCNPs@Zn_xCd_{1-x}S yolk-shell nanoparticles at 345, 360, 451, 476, 520 and 543 nm, respectively.

formation of yolk-shell nanostructure and close combination of UCNPs and Zn_xCd_{1-x}S.

Fig. 4b shows the UV-vis absorption spectra of the as-prepared different samples, the as-prepared UCNPs@Zn_xCd_{1-x}S yolk-shell nanoparticles exhibit stronger UV-vis absorption at 400–600 nm, enhancing the overlap of the fluorescence spectra of UCNPs and the absorption spectra of Zn_xCd_{1-x}S, which will result in the reduced photoluminescence (PL) emissions of UCNPs via fluorescence resonance energy transfer process and the increased hydroxyl radical (·OH) generation amount of Zn_xCd_{1-x}S under irradiation of NIR light [47,51]. The

band gap energies of the as-prepared yolk-shell nanoparticles at 300 K have been evaluated from the UV-vis diffuse reflectance spectra (DRS) and Kubelka-Munk Plots derived from the Kubelka-Munk function [F(R) $h\nu$]² versus photon energy ($h\nu$) (Fig. 4c-d) [47]. As shown in Table S2 (supporting information), the estimated band gap energies of the as-prepared UCNPs@Zn_xCd_{1-x}S ($x = 1, 0.45, 0.35, 0.28$) nanoparticles are 3.49, 2.40, 2.375, 2.345 eV, respectively, further verifying the formation of alloyed shell layers. The dynamic luminescence spectra (Fig. 5a-f) show the luminescence lifetime of the excited state levels of Tm³⁺ (Fig. 5a-d) and Er³⁺ (Fig. 5e,f) are greatly shortened, which

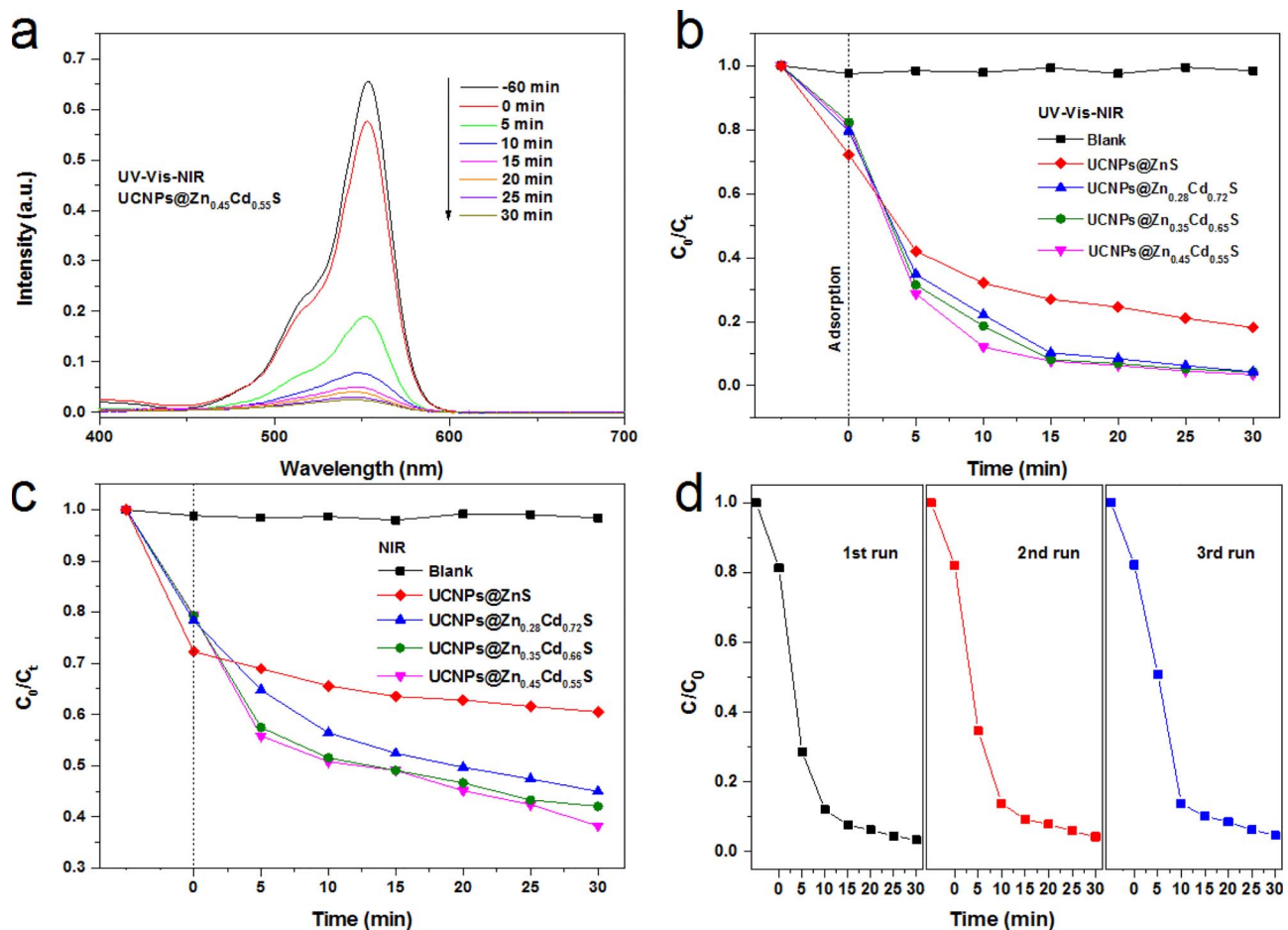


Fig. 6. (a) UV-vis absorbance spectra of RhB solution show the photodecomposition of the RhB dyes in solution (5.0 mg/L, 50 mL) over 15 mg UCNPs@Zn_{0.45}Cd_{0.55}S at given irradiation times under irradiation of a 1500 mW Xe lamp. (b) Evolution of RhB concentration versus irradiation time in the presence of different UCNPs@Zn_xCd_{1-x}S photocatalysts under irradiation of a simulated solar light, where C₀ and C_t are the concentration of initial solution and the concentration at the given irradiation time t (min), respectively. (c) Evolution of RhB concentration versus irradiation time in the absence and presence of UCNPs@Zn_xCd_{1-x}S nanoparticles (x = 0.28, 0.35, 0.45) under irradiation of a simulated solar light with a UV-vis filter, where C₀ and C_t are the concentration of initial solution and the concentration at the irradiation time t (min), respectively. During the photocatalysis reaction, the UCNPs@Zn_xCd_{1-x}S nanoparticles (x = 0.28, 0.35, 0.45) were incubated with RhB solution after equilibrium for 1 h before the light irradiation. (d) The recycling activity for the UCNPs@Zn_{0.45}Cd_{0.55}S yolk-shell nanoparticles.

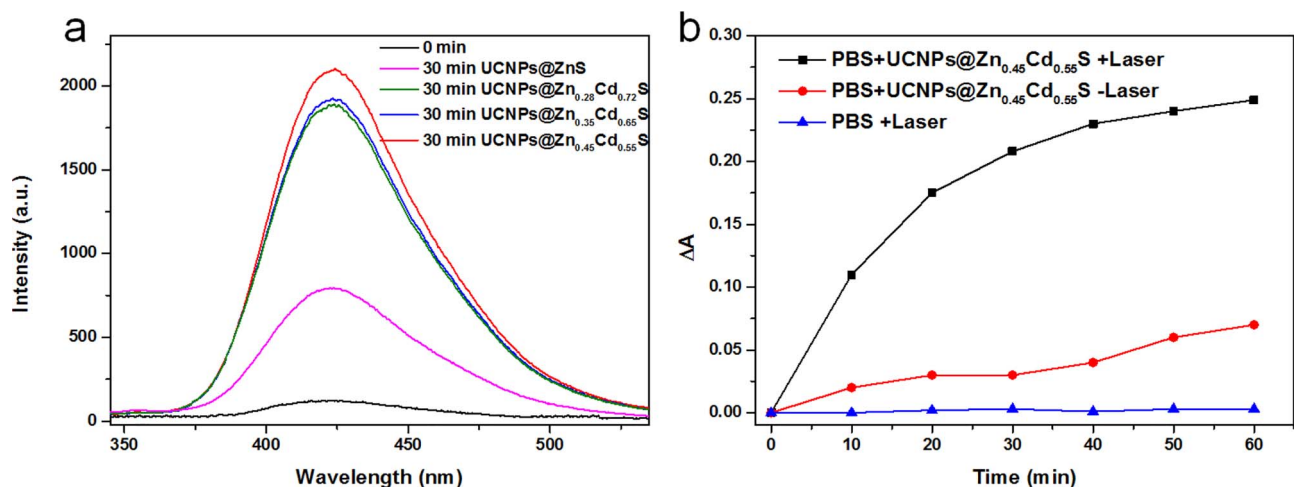
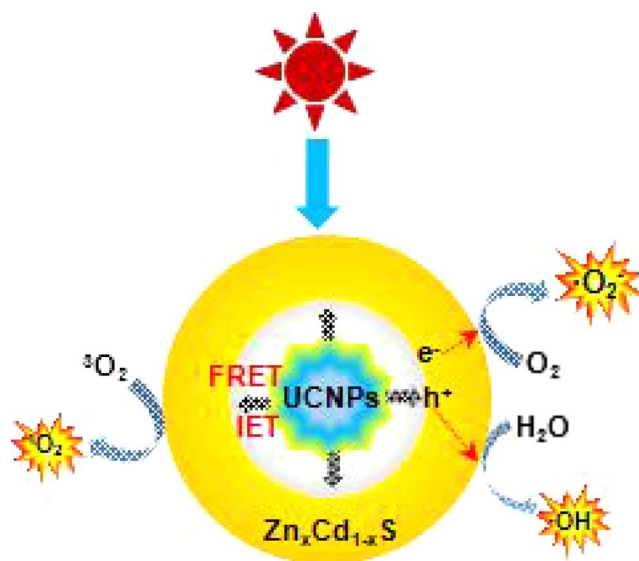


Fig. 7. (a) Fluorescence spectra of terephthalic acid (TAOH) with the addition of UCNPs@Zn_xCd_{1-x}S (x = 0.28, 0.35, 0.45) nanoparticles excited by a 980 nm CW laser. (b) The absorption intensity changing at 380 nm for 9, 10-Anthracenediyl-bis (methylene) dimalonic acid (ABDA) under excited using a Xe lamp equipped with an UV-vis filter, illustrating the production of singlet oxygen (¹O₂).



Scheme 1. Illustration of the photocatalysis mechanism under irradiation of NIR light.

confirmed that the highly efficient fluorescence resonance energy transfer process or irradiation energy transfer (IET) process was happened between the FRET donors and the acceptors [52–55]. Based on the above analysis, as expected, the as-prepared samples show better photocatalytic ability owing to higher energy transfer efficiency.

Degradation of rhodamine B (RhB) dyes was chosen as a model to investigate the photocatalytic performance. Fig. 6a, b show that 90% of dyes (50 mL, 5.0 mg/L) have been degraded in 10 min in the presence of 15 mg UCNPs@Zn_{0.45}Cd_{0.55}S nanoparticles under irradiation of the lamp without any filters. In contrast, 65% of RhB dyes molecules have been decomposed in 30 min with the same condition (Fig. 6c), under irradiation of NIR light using a Xe lamp equipped with an UV-vis filter. It's noticed that the as-prepared yolk-shell nanoparticles of UCNPs@Zn_{0.45}Cd_{0.55}S show better photocatalytic performance on degradation towards RhB dyes compared to the nanostructures of UCNPs@Zn_{0.28}Cd_{0.72}S and UCNPs@Zn_{0.35}Cd_{0.65}S. The as-prepared UCNPs@Zn_{0.45}Cd_{0.55}S yolk-shell nanoparticles shows the weakest fluorescence emission under 360 nm excitation, illustrating the highest separated efficiency of the photo-generated electron and positive hole in this work (Fig. S6, supporting information) [56]. Therefore, the as-prepared UCNPs@Zn_xCd_{1-x}S yolk-shell nanoparticles show excellent photocatalytic ability, which can be attributed to the efficiently separation efficiency between the photo-generated electron-hole pairs. In addition, the as-prepared UCNPs@Zn_{0.45}Cd_{0.55}S yolk-shell nanoparticles exhibit excellent chemical stability after used for three cycles (Fig. 6d).

Fig. 7a shows that the fluorescence spectra of terephthalic acid (TAOH) in the presence of UCNPs@Zn_xCd_{1-x}S nanoparticles excited by a 980 nm CW laser, in which a strong fluorescence peak were observed, demonstrating the production of a large amount of ·OH. A large amount of singlet oxygen species also have been observed under irradiation of NIR light (Fig. 7b). The hydroxyl radical (·OH) and single oxygen (¹O₂) produced by NIR light can be used to kill cancer cells and photodegrade towards organic dyes for making full use of solar energy [57–60]. The photocatalysis mechanism has been summarized in Scheme 1. As shown in Scheme 1, NIR light from solar energy can activate UCNPs, the excited UCNPs which can further activate the Zn_xCd_{1-x}S nanoparticles via FRET or IET process to produce photo-generated electron and positive hole, which will result in the formation of lots of hydroxyl radical (·OH) and single oxygen (¹O₂) to render the decomposition of organic dyes including RhB. In particular, the as-prepared UCNPs@Zn_{0.45}Cd_{0.55}S yolk-shell nanoparticles show excellent biocompatibility, even though the concentration of the nanoparticles was up to 400 µg/L (Fig. S7, Supporting Information), which is of great importance for

wide applications in wastewater treatment, bionanotechnology including cancer treatment and etc. In vitro photodynamic therapy of cancer cells has been carried out, which demonstrated that the cell viabilities of Hela cells would significantly decrease as either the concentration of UCNPs@Zn_{0.45}Cd_{0.55}S or NIR laser irradiation time increased. (Fig. S8, Supporting Information)

4. Conclusions

In summary, a facile template-assisted hydrothermal process has been developed to fabricate yolk-shell nanoparticles of UCNPs@Zn_xCd_{1-x}S using UCNPs@ZnS core-shell nanoparticles as hard template. To gain better understanding of the growth mechanism of yolk-shell nanostructures, the shape evolution with the time has been extensively investigated. The amount of Cd(Ac)₂ plays an important role in the formation of this kind of nanostructures. The steady and dynamic state fluorescence spectra of the as-prepared UCNPs@Zn_xCd_{1-x}S nanoparticles verify that the highly efficient energy transfer between the UCNPs and Zn_xCd_{1-x}S has been achieved. In the present study, the as-prepared UCNPs@Zn_xCd_{1-x}S nanoparticles show excellent biocompatibility, excellent photocatalytic ability and high production of hydroxyl radical (·OH) and single oxygen (¹O₂). Therefore, this work should provide an alternative nanoparticle for important and potential applications in energy conversion, bionanotechnology, wastewater treatment and etc.

Acknowledgments

We acknowledge the funding supports from the National Natural Science Foundation of China (Grant 21471043). W. Wang and C. Huang contributed equally to this work.

Appendix A. Supplementary data

Supplementary data associated with this article can be found, in the online version, at <http://dx.doi.org/10.1016/j.apcatb.2017.11.037>.

References

- [1] A. Fujishima, K. Honda, *Nature* 238 (1972) 37–38.
- [2] W. Wang, M.Y. Ding, C.H. Lu, Y.R. Ni, Z.Z. Xu, *Appl. Catal. B-Environ.* 144 (2014) 379–385.
- [3] X.H. Liu, W.H. Di, W.P. Qin, *Appl. Catal. B-Environ.* 205 (2017) 158–164.
- [4] Y.H. Sang, Z.H. Zhao, M.W. Zhao, P. Hao, Y.H. Leng, H. Liu, *Adv. Mater.* 27 (2016) 363–369.
- [5] J.B. Cui, Y.J. Li, L. Liu, L. Chen, J. Xu, J.W. Ma, G. Fang, E.B. Zhu, H. Wu, L.X. Zhao, L.Y. Wang, Y. Huang, *Nano Lett.* 15 (2015) 6295–6301.
- [6] Y.F. Shi, C.X. Hu, B. Li, X.P. Fang, C.H. Yao, Y.C. Zhang, Y.S. Hu, Z.X. Wang, L.Q. Chen, D.Y. Zhao, G.D. Stucky, *Adv. Funct. Mater.* 23 (2013) 1832–1838.
- [7] S. Shanmugam, J.T. Xu, C. Boyer, *Angew. Chem. Int. Ed.* 55 (2016) 1036–1040.
- [8] F. Wang, Y. Han, C.S. Lim, Y.H. Lu, J. Wang, J. Xu, H.Y. Chen, C. Zhang, M.H. Hong, X.G. Liu, *Nature* 463 (2010) 1061–1065.
- [9] F. Wang, R.R. Deng, J. Wang, Q.X. Wang, Y. Han, H.M. Zhu, X.Y. Chen, X.G. Liu, *Nat. Mater.* 10 (2011) 968–973.
- [10] H. Dong, L.D. Sun, Y.F. Wang, J. Ke, R. Si, J.W. Xiao, G.M. Lyu, S. Shi, C.H. Yan, *J. Am. Chem. Soc.* 137 (2015) 6569–6576.
- [11] Y.X. Liu, D.S. Wang, J.X. Shi, Q. Peng, Y.D. Li, *Angew. Chem. Int. Ed.* 52 (2013) 4366–4369.
- [12] N.M. Idris, M.K. Gnansammandhan, J. Zhang, P.C. Ho, R. Mahendran, Y. Zhang, *Nat. Med.* 18 (2012) (1580-U190).
- [13] J. de Wild, A. Meijerink, J.K. Rath, W.G.J.H.M. van Sark, R.E.I. Schropp, *Energ. Environ. Sci.* 4 (2011) 4835–4848.
- [14] W.H. Feng, B. Wang, Z.Y. Zheng, Z.B. Fang, Z.F. Wang, S.Y. Zhang, Y.H. Li, P. Liu, *Appl. Catal. B-Environ.* 186 (2016) 143–150.
- [15] W. Zheng, P. Huang, D.T. Tu, E. Ma, H.M. Zhu, X.Y. Chen, *Chem. Soc. Rev.* 44 (2015) 1379–1415.
- [16] J. Zhou, Q. Liu, W. Feng, Y. Sun, F.Y. Li, *Chem. Rev.* 115 (2015) 395–465.
- [17] W.W. Ye, M.K. Tsang, X. Liu, M. Yang, J.H. Hao, *Small* 10 (2014) 2390–2397.
- [18] P. Huang, W. Zheng, S.Y. Zhou, D.T. Tu, Z. Chen, H.M. Zhu, R.F. Li, E. Ma, M.D. Huang, X.Y. Chen, *Angew. Chem. Int. Ed. It.* 53 (2014) 1252–1257.
- [19] F. Carmona, M. Poli, M. Bertuzzi, A. Gianoncelli, F. Gangemi, P. Arosio, *BBA-Gen. Subj.* 1861 (2017) 522–532.
- [20] J.E. Ghadiali, B.E. Cohen, M.M. Stevens, *ACS Nano* 4 (2010) 4915–4919.
- [21] R. Tsukanov, T.E. Tomov, M. Liber, Y. Berger, E. Nir, *Acc. Chem. Res.* 47 (2014)

1789–1798.

[22] Q.Q. Zhan, J. Qian, H.J. Liang, G. Somesfalean, D. Wang, S.L. He, Z.G. Zhang, S. Andersson-Engels, *ACS Nano* 5 (2011) 3744–3757.

[23] S. Wu, H.J. Butt, *Adv. Mater.* 28 (2016) 1208–1226.

[24] L. Wang, H. Dong, Y.N. Li, R. Liu, Y.F. Wang, H.K. Bisoyi, L.D. Sun, C.H. Yan, Q. Li, *Adv. Mater.* 27 (2015) 2065–2069.

[25] Y.B. Wang, B.N. Si, S.W. Lu, E.Z. Liu, X.Y. Hu, J. Fan, *Sensor Actuat. B-Chem.* 246 (2017) 127–135.

[26] D. Wang, B. Xue, X.G. Kong, L.P. Tu, X.M. Liu, Y.L. Zhang, Y.L. Chang, Y.S. Luo, H.Y. Zhao, H. Zhang, *Nanoscale* 7 (2015) 190–197.

[27] M. Lin, Y. Gao, T.J. Diefenbach, J.K. Shen, F.J. Hornicek, Y.I. Park, F. Xu, T.J. Lu, M. Amiji, Z.F. Duan, *A.C.S. Appl. Mater. Interfaces.* 9 (2017) 7941–7949.

[28] X. Wu, Y.W. Zhang, K. Takle, O. Bilsel, Z.J. Li, H. Lee, Z.J. Zhang, D.S. Li, W. Fan, C.Y. Duan, E.M. Chan, C. Lois, Y. Xiang, G. Han, *ACS Nano* 10 (2016) 1060–1066.

[29] R.C. Lv, P.P. Yang, F. He, S.L. Gai, C.X. Li, Y.L. Dai, G.X. Yang, J. Lin, *ACS Nano* 9 (2015) 1630–1647.

[30] G. Tian, W.L. Ren, L. Yan, S. Jian, Z.J. Gu, L.J. Zhou, S. Jin, W.Y. Yin, S.J. Li, Y.L. Zhao, *Small* 9 (2013) 1929–1938.

[31] N.N. Li, X.Y. Wen, J. Liu, B.J. Wang, Q.Q. Zhan, S.L. He, *Opt. Mater. Express* 6 (2016) 1161–1171.

[32] F.Y. Liu, Q. Zhao, H.P. You, Z.X. Wang, *Nanoscale* 5 (2013) 1047–1053.

[33] Z.Y. Hou, C.X. Li, P.A. Ma, G.G. Li, Z.Y. Cheng, C. Peng, D.M. Yang, P.P. Yang, J. Lin, *Adv. Funct. Mater.* 21 (2011) 2356–2365.

[34] A. Bednarkiewicz, M. Nyk, M. Samoc, W. Strek, *J. Phys. Chem. C* 114 (2010) 17535–17541.

[35] C.H. Li, F. Wang, J.A. Zhu, J.C. Yu, *Appl. Catal. B-Environ.* 100 (2010) 433–439.

[36] C.Z. Yuan, G.Y. Chen, L. Li, J.A. Damasco, Z.J. Ning, H. Xing, T.M. Zhang, L.C. Sun, H. Zeng, A.N. Cartwright, P.N. Prasad, H. Agren, *A.C.S. Appl. Mater. Interfaces* 6 (2014) 18018–18025.

[37] W. Wang, M.Y. Ding, C.H. Lu, Y.R. Ni, Z.Z. Xu, *Appl. Catal. B-Environ.* 144 (2014) 379–385.

[38] S.S. Lucky, N.M. Idris, Z.Q. Li, K. Huang, K.C. Soo, Y. Zhang, *ACS Nano* 9 (2015) 191–205.

[39] F. Zhang, C.L. Zhang, H.Y. Peng, H.P. Cong, H.S. Qian, *Part. Part. Syst. Char.* 33 (2016) 248–253.

[40] F. Zhang, W.N. Wang, H.P. Cong, L.B. Luo, Z.B. Zha, H.S. Qian, *Part. Part. Syst. Char.* 34 (2017) 1600222.

[41] F. Zhang, C.L. Zhang, W.N. Wang, H.P. Cong, H.S. Qian, *ChemSusChem* 9 (2016) 1449–1454.

[42] F. Zhang, L.N. Hao, Y. Wang, S. Cheng, W.N. Wang, C.L. Zhang, F. Xu, H.S. Qian, *CrystEngComm* 18 (2016) 6013–6018.

[43] H.B. Shen, W.R. Cao, N.T. Shewmon, C.C. Yang, L.S. Li, J.G. Xue, *Nano Lett.* 15 (2015) 1211–1216.

[44] Y.G. Chen, S. Zhao, X. Wang, Q. Peng, R. Lin, Y. Wang, R.A. Shen, X. Cao, L.B. Zhang, G. Zhou, J. Li, A.D. Xia, Y.D. Li, *J. Am. Chem. Soc.* 138 (2016) 4286–4289.

[45] B.B. Ding, H.Y. Peng, H.S. Qian, L. Zheng, S.H. Yu, *Adv. Mater. Interfaces* 3 (2016) 1500649.

[46] H.Y. Fan, E. Leve, J. Gabaldon, A. Wright, R.E. Haddad, C.J. Brinker, *Adv. Mater.* 17 (2005) 2587–2590.

[47] J. Chen, B.B. Ding, T.Y. Wang, F. Li, Y. Zhang, Y.L. Zhao, H.S. Qian, *J. Mater. Sci.-Mater. El.* 25 (2014) 4103–4109.

[48] P.L. Huang, B.Z. Zeng, Z.X. Mai, J.T. Deng, Y.P. Fang, W.H. Huang, H.W. Zhang, J.Y. Yuan, Y. Wei, W.Y. Zhou, *Mater. Chem. B* 4 (2016) 46–56.

[49] N. Zhang, X.Z. Fu, Y.J. Xu, *Mater. Chem. B* 21 (2011) 8152–8158.

[50] F.B. Gu, H.H. Chen, D.M. Han, Z.H. Wang, *RSC. Adv.* 6 (2016) 29727–29733.

[51] D.H. Wang, L. Wang, A.W. Xu, *Nanoscale* 4 (2012) 2046–2053.

[52] S. Cimitan, S. Albonetti, L. Forni, F. Peri, D. Lazzari, *J. Colloid Interf. Sci.* 329 (2009) 73–80.

[53] H.C. Liu, M.K.G. Jayakumar, K. Huang, Z. Wang, X. Zheng, H. Agren, Y. Zhang, *Nanoscale* 9 (2017) 1676–1686.

[54] K. Huang, N.M. Idris, Y. Zhang, *Small* 12 (2016) 836–852.

[55] P.Y. Qiu, N. Zhou, H.Y. Chen, C.L. Zhang, G. Gao, D.X. Cui, *Nanoscale* 5 (2013) 11512–11525.

[56] W.L. Yang, L. Zhang, Y. Hu, Y.J. Zhong, H.B. Wu, X.W. Lou, *Angew. Chem. Int. Ed.* 51 (2012) 11501–11504.

[57] Y.H. Wang, H.G. Wang, D.P. Liu, S.Y. Song, X. Wang, H.J. Zhang, *Biomaterials* 34 (2013) 7715–7724.

[58] M.H. Li, Z.J. Zheng, Y.Q. Zheng, C. Cui, C.X. Li, Z.Q. Li, *A.C.S. Appl. Mater. Interfaces* 9 (2017) 2899–2905.

[59] Y.T. Zhong, G. Tian, Z.J. Gu, Y.J. Yang, L. Gu, Y.L. Zhao, Y. Ma, J.N. Yao, *Adv. Mater.* 26 (2014) 2831–2837.

[60] W.N. Wang, F. Zhang, C.L. Zhang, Y.C. Guo, W. Dai, H.S. Qian, *ChemCatChem* 9 (2017) 3611–3617.